

Experiments with high-energy neutrino beams*

J. Steinberger

CERN, CH-1211 Geneva, Switzerland
and Scuola Normale Superiore, 56100 Pisa, Italy

1. INTRODUCTION

High-energy neutrino beams have found intensive and varied application in particle physics experimentation in the last decades. This review is constrained to a few of the most fruitful examples: the discovery of neutral currents, the measurement of the Weinberg angle, the study of weak currents and the consequent test of the electroweak theory, the study of nucleon quark structure, and the testing of quantum chromodynamics (QCD). Other studies, such as the production of “prompt” neutrinos, the search for finite neutrino masses and neutrino oscillations, the search for heavy leptons or other new particles, or the measurement of proton and neutron structure functions, elastic and pseudoelastic cross sections, and other exclusive processes, are not discussed here. Neutrino experiments have been pursued vigorously at the Brookhaven National Laboratory, at Fermilab, and at CERN. It is fair to say that they have made large contributions to our understanding of particle physics.

2. NEUTRINO BEAMS

Present neutrino beams are produced in four steps: (i) production of secondary hadrons in the collision of high-energy protons on a fixed target; (ii) momentum (charge) selection and focusing of the hadrons; (iii) passage of the beam through an (evacuated) decay region, long enough to permit a substantial fraction of the hadrons to decay; (iv) absorption of the remaining hadrons and the muons that are produced along with the neutrinos in a shield of adequate thickness. The two-body decays $\pi^{+(-)} \rightarrow \mu^{+(-)} + \nu(\bar{\nu})$ and $K^{+(-)} \rightarrow \mu^{+(-)} + \nu(\bar{\nu})$ account for $\sim 97\%$ of the neutrino flux in present beams. Positive hadrons produce neutrinos, negative hadrons produce antineutrinos. Figures 1(a) and 1(b) give an impression of the two hadron beam-forming options that are available, side by side, at CERN: a conventional, so-called narrow-band beam (NBB), and an achromatic, Van der Meer horn-focused, wide-band beam (WBB). The neutrino spectra produced by these two beams are very different, as shown in Fig. 2. The WBB's are characterized by high intensity, a steep (generally undesirable) energy falloff, and a substantial contamination of “wrong sign” neutrinos. The NBB's have lower intensity, a flat

energy dependence in the contribution from each of the two decays, and small wrong-sign background. They also have the important feature that the energy of the neutrino can be known, subject to a twofold π - K dichotomy, if the decay angle is known. In general this can be inferred from the impact parameter of the event in the detector.

3. DETECTORS

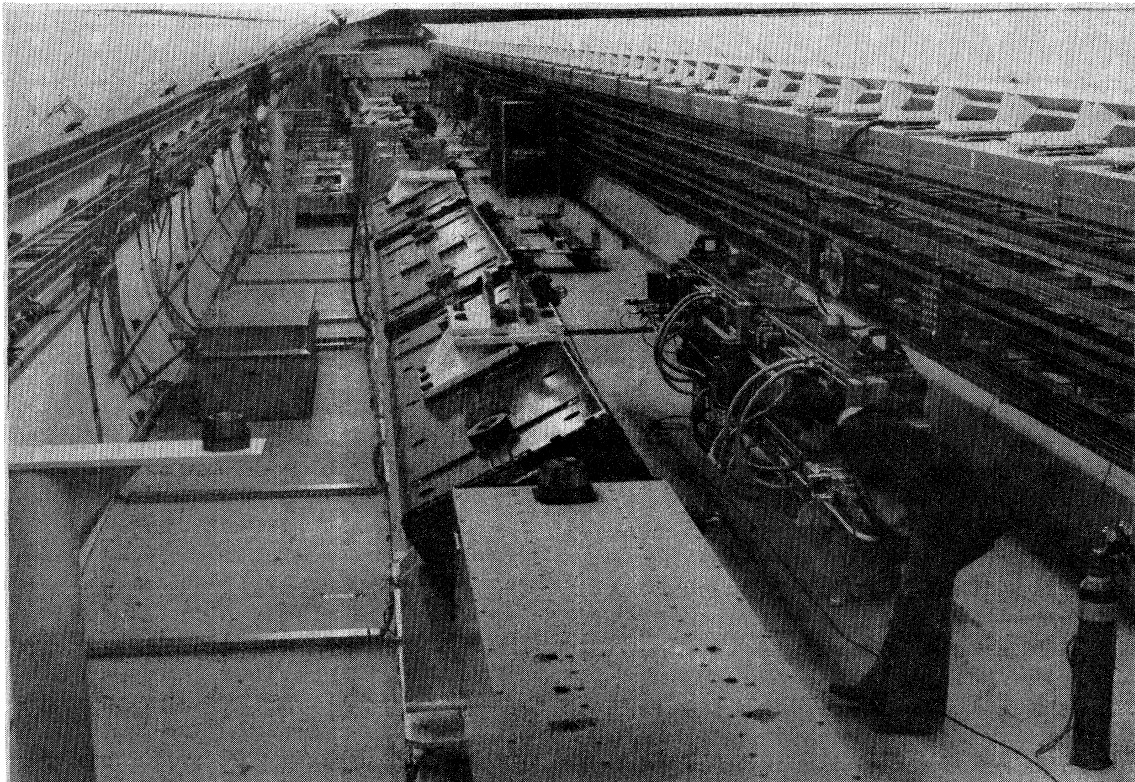
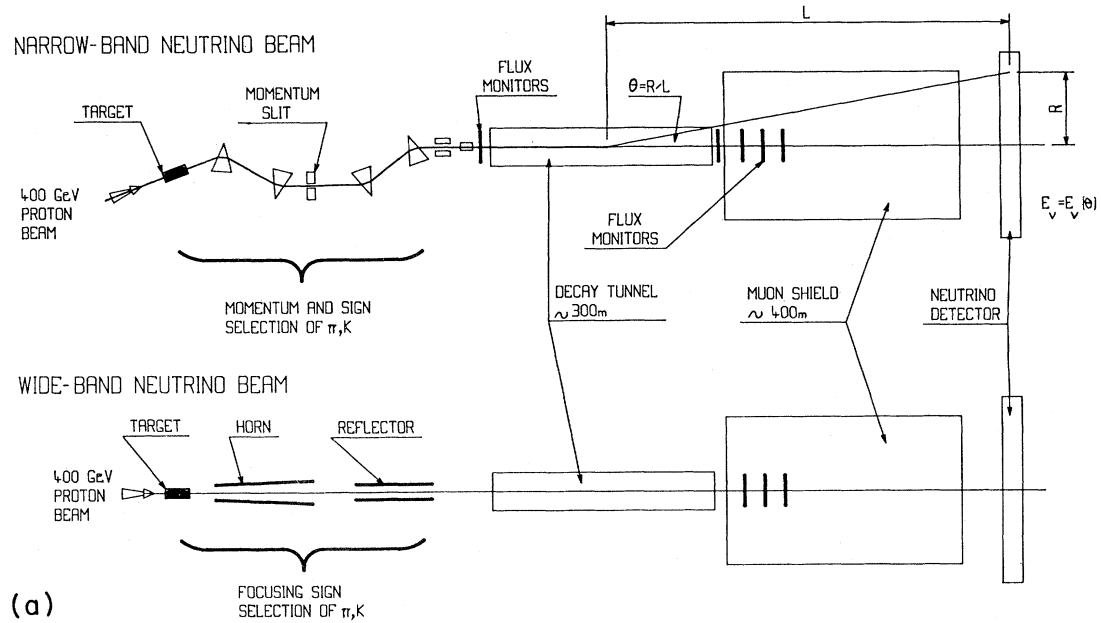
The low cross sections of neutrinos are reflected in two general features of neutrino detectors: (i) they are massive; (ii) the target serves also as detector.

In the seventies, the most successful detectors were large bubble chambers. The most splendid of these were the cryogenic devices built at CERN and Fermilab, each with a volume of $\sim 15 \text{ m}^3$, in large magnetic fields, and each capable of operating with liquid hydrogen, deuterium, or neon. A picture of a typical neutrino event in the CERN chamber is shown in Fig. 3. It is an example of the “charged-current” (CC) reaction $\nu + N \rightarrow \mu^- + \text{hadrons}$. However, one of the major discoveries at CERN was made not in this but in a large Freon-filled bubble chamber, affectionately called Gargamelle. The active volume was a cylinder 4.8 m long and 1.9 m in diameter, for a volume of about 13 m^3 , inside a magnet producing a field of 2 T. Figure 4 gives some impression of its size.

The bubble chamber has now been largely replaced by detectors based on electronic detection methods. As an example, I mention here the CDHS (CERN-Dortmund-Heidelberg-Saclay Collaboration) detector used at CERN from 1977 to 1985. It consists of 19 modules made of iron plates 3.75 m in diameter, each with total iron thickness of 75 cm and a weight of ~ 65 tons. The iron is toroidally magnetized to a field of 1.7 T by means of coils that pass through a hole in the center.

Interleaved with the 5-cm-thick iron plates are scintillator strips, which serve to measure the energy of the secondary hadrons by sampling the ionization. The typical hadron shower is ~ 25 cm in radius and ~ 1 m long, so the shower dimensions are very small compared with the size of the detector. The muon momenta are determined on the basis of curvature in the magnetic field, with the help of drift chambers inserted between the iron modules. These measure the positions of traversing tracks in three projections. The useful target weight is ~ 800 tons. Figure 5 shows the CDHS experiment and Fig. 6 a typical event of the same type as that shown in Fig. 3.

*This lecture was delivered 8 December 1988, on the occasion of the presentation of the 1988 Nobel Prize in Physics.



(b)

FIG. 1. (a) Sketch of narrow-band and wide-band neutrino beam layouts at CERN, showing disposition of primary target, focusing elements, decay region, shielding, and monitoring devices. (b) View of the neutrino beam tunnel at the CERN SPS in 1976, before operations began. The NBB line is seen in the center; on the right is the pulse transformer for the WBB horn, but the horn itself, destined for the pedestal on the left, is not yet installed. At the far end, the 2.5-m-diameter titanium window of the evacuated decay region can be seen. Photograph by PHOTO CERN.

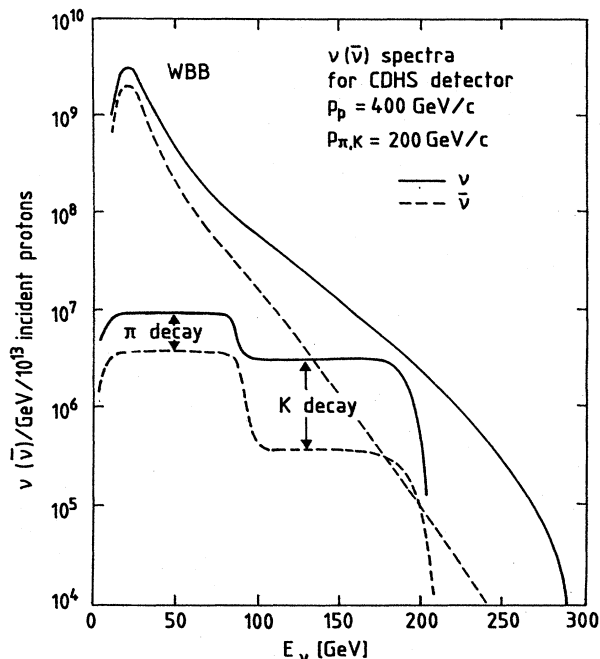


FIG. 2. Neutrino and antineutrino energy spectra, calculated for the horn-focused WBB and the more conventional NBB.



FIG. 3. A typical neutrino event as observed in the Big European Bubble Chamber (BEBC) filled with neon at the CERN 450-GeV Super Proton Synchrotron (SPS) accelerator. The muon can be seen on the left. It has been tagged by an external muon identifier. The many-particle hadron shower is to the right. Photograph by PHOTO CERN.

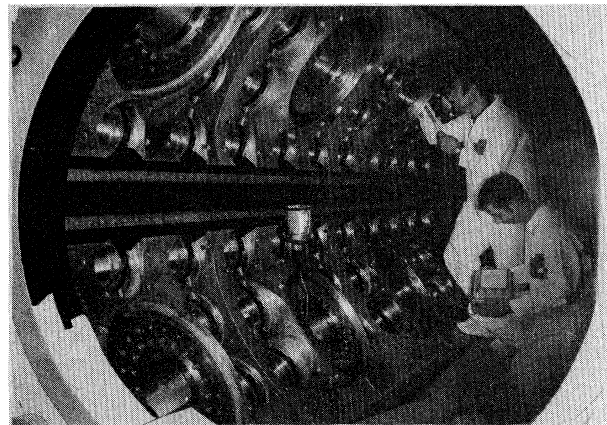


FIG. 4. Preparation of the interior of the 13-m³ bubble chamber Gargamelle, later to be filled with Freon. It is with this detector that the neutral currents were discovered. Photograph by PHOTO CERN.

4. NEUTRAL CURRENTS

4.1 Discovery

The evolution of the electroweak unified gauge theory in the late sixties and early seventies was a miraculous achievement, but one that had no immediate impact on the majority of particle physicists—certainly not on me—perhaps because it was a theoretical construct which left the existing experimental domain intact. However, it predicted some entirely new phenomena, and of these the neutral weak currents were the first to be discovered. The verification of neutral currents (NC's) established the theory overnight, and subsequent experiments on their detailed structure reinforced this. This observation (Hasert *et al.*, 1973b) of neutral weak currents at CERN in 1973 by the Gargamelle group was the first great discovery made at CERN. It was followed 10 years later by the second—also a prediction of the same theory—the intermediate boson.

The bubble chamber, built under the direction of A. Lagarrigue at the École Polytechnique in Paris, was exposed to neutrino and antineutrino WBB's at the CERN 24-GeV proton accelerator. The normal CC reactions,

$$\nu(\bar{\nu}) + N \rightarrow \mu^-(\mu^+) + \text{hadrons} ,$$

were found as usual, but NC “muonless” reactions,

$$\nu(\bar{\nu}) + N \rightarrow \nu(\bar{\nu}) + \text{hadrons} ,$$

which had hardly been looked for before—and therefore had not been found—were there as well. Such an event is shown in Fig. 7. These events were selected on the basis of there being no muon candidate among the observed particles. The main experimental challenge was to show that they were not due to stray neutrons in the beam. I

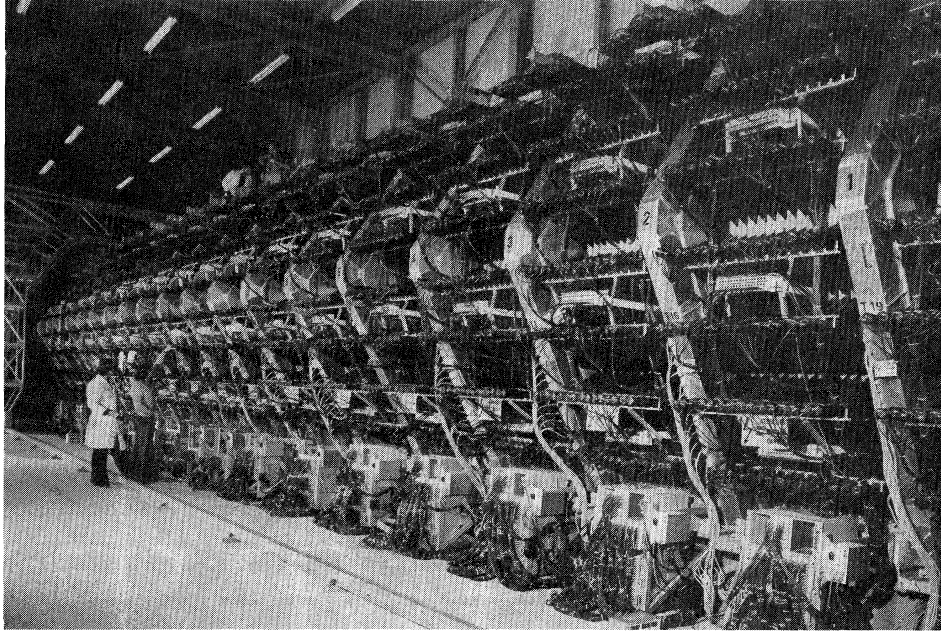


FIG. 5. View along the 19 modules of the CDHS electronic neutrino detector at the SPS. The black light-guides and phototubes, which are used to measure the hadron energy, can be seen sticking out of the magnetized iron modules. The hexagonal aluminum structures are the drift chambers that measure the muon trajectories. Photograph by PHOTO CERN.

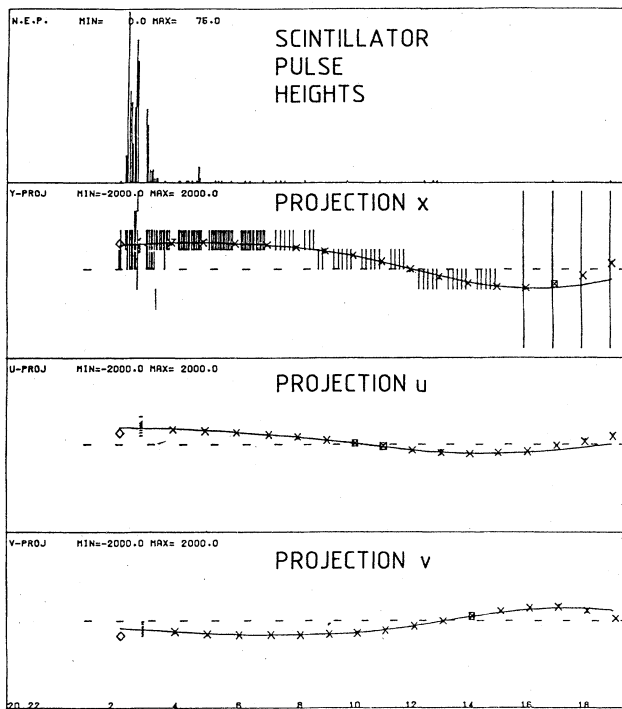


FIG. 6. Computer reconstruction of a typical event of the reaction $\nu + \text{Fe} \rightarrow \mu^- + X$. Four views are shown, with the horizontal axis along the beam direction. The top view shows the scintillator pulse height, or hadron energy, and its distribution along the detector. The next view shows the scintillator hits as well as the horizontal wire hits and the reconstructed track in the x projection. The other two views show the wire hits and the reconstructed track for the $\pm 60^\circ$ projections.

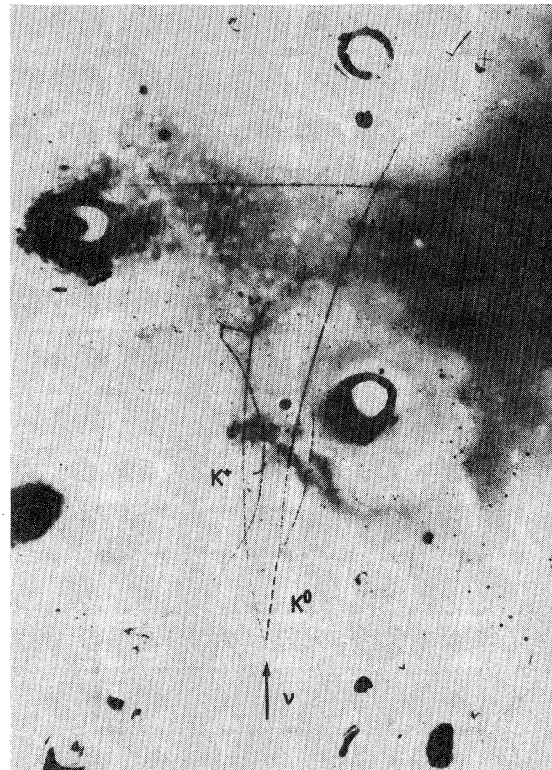


FIG. 7. A "muonless" event in Gargamelle. All tracks stop or interact in the chamber. None could be a muon. The neutrino produces one K^+ and one K^0 meson. The K^+ meson interacts in the liquid and then decays. The invisible K^0 meson decays to two pions.

myself was a sceptic for a long time, and I lost a bottle or two of good wine on this matter. However, the neutron background would be expected to decrease exponentially along the length of the chamber, roughly with the neutron mean free path in Freon. Instead, the event distribution was flat, as expected for neutrino events (see Fig. 8). I have never enjoyed paying up a debt more than at the dinner we gave for the winners, very good friends, Jacques Prentki, John Iliopoulos, and Henri Epstein.

The ratios of the cross sections

$$R_\nu = \frac{\sigma_\nu^{\text{NC}}}{\sigma_\nu^{\text{CC}}} \quad \text{and} \quad R_{\bar{\nu}} = \frac{\sigma_{\bar{\nu}}^{\text{NC}}}{\sigma_{\bar{\nu}}^{\text{CC}}}$$

are given in the electroweak theory in terms of the Weinberg angle θ_W :

$$R_\nu = \frac{1}{2} - \sin^2\theta_W + (1+r)\frac{5}{9}\sin^4\theta_W \quad (1)$$

and

$$R_{\bar{\nu}} = \frac{1}{2} - \sin^2\theta_W + (1+1/r)\frac{5}{9}\sin^4\theta_W, \quad (2)$$

where r is the ratio of antineutrino to neutrino CC total cross sections: $r = \sigma^{\text{CC},\bar{\nu}}/\sigma^{\text{CC},\nu} = 0.48 \pm 0.02$ experimentally. On the basis of these ratios, the experiment yielded

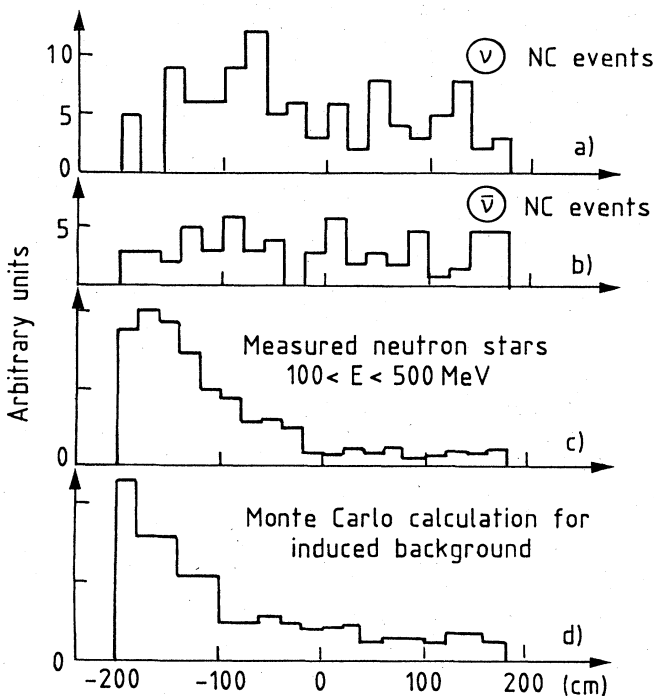


FIG. 8. Distribution of the origin of muonless events along the beam direction in Gargamelle. Neutrino events are expected to be uniformly distributed, whereas neutron events should decrease with distance because of their absorption in the Freon. The nuclear mean free path in Freon is about 80 cm. The expected and observed distributions of neutron interactions are shown in the bottom two histograms. The muonless events are consistent with neutrino and inconsistent with neutron origin (Hasert *et al.*, 1973b).

a first measure of $\sin^2\theta_W$ that was not very different from present, more precise determinations. In the same exposure a beautiful example of another NC process, the scattering of an antineutrino on an electron, was also found (Hasert *et al.*, 1973a).

4.2 Precision measurement of $\sin^2\theta_W$

The higher energies that became available a few years later at Fermilab and CERN made the study of NC processes much easier. The muons of the CC background had now a greater penetration power, which permitted cleaner separation of NC and CC events. Moreover, with the advent of the higher energies, the advantage in the study of inclusive neutrino scattering had shifted to electronic detection techniques. In the period 1977 to 1985, hadronic NC neutrino scattering was studied extensively by the CDHS Collaboration at CERN in order to get a more precise value for θ_W (Holder *et al.*, 1977b; Abramowicz *et al.*, 1985, 1986) and to check the prediction of the electroweak theory for the ratio of right-handed to left-handed NC's (Holder *et al.*, 1977c). The NC events are selected on the basis of short event length, i.e., the short penetration of the hadronic shower compared with that of the muon of CC events. This is illustrated in Fig. 9. A 15% background of CC events is subtracted. The neutrino NC-to-CC ratio R_ν yielded the most precise value of the weak mixing angle available to date, $\sin^2\theta_W = 0.227 \pm 0.006$. Once $\sin^2\theta_W$ is known, the antineutrino ratio $R_{\bar{\nu}}$ follows from Eq. (2). Its measurement provided a sensitive test of the electroweak theory and confirmed it in its simplest form. The presence of right-handed NC's (CC's are purely left-handed) in the amount predicted by the theory could be demonstrated by comparing the hadron energy distributions of the NC and CC processes. The result is shown in Fig. 10.

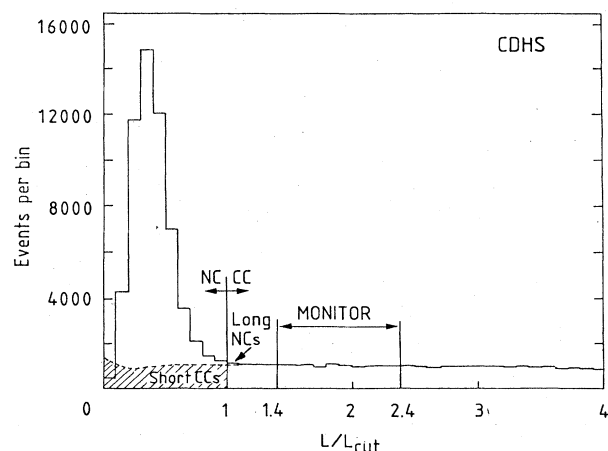


FIG. 9. Identification, by the CDHS Collaboration, of neutral-current (NC) events by their short event length. The peak at small event lengths is due to NC events. The long tail is due to muonic events, which must be subtracted under the peak to give the NC rate (Holder *et al.*, 1977b; Abramowicz *et al.*, 1985, 1986).

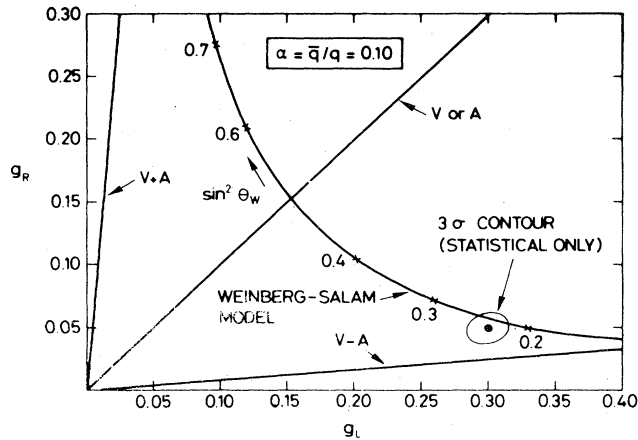


FIG. 10. Strengths of the left- and right-handed neutral currents. If the NC were purely left handed, as is the case for the CC, the experimental point would be expected to fall on the $V - A$ line. The experiment shows a right-handed component, which is just that expected in the electroweak theory (Weinberg-Salam model) (Holder *et al.*, 1977c).

4.3 Neutrino-electron scattering

The elastic-scattering reactions of neutrinos on atomic electrons,

$$\nu_\mu + e^- \rightarrow \nu_\mu + e^- \quad \text{and} \quad \bar{\nu}_\mu + e^- \rightarrow \bar{\nu}_\mu + e^- ,$$

proceed via NC's. They are characterized by small cross sections—smaller than their hadronic counterparts by the mass ratio m_e/m_p because of the smaller c.m. energies—and, for the same reason, by small electron production angles, $\theta_e \approx \sqrt{m_e/E_\nu}$. Until now, these angles have not been resolved by the experiments, so only total cross sections have been measured. The expectations in the electroweak theory are

$$\sigma^{\nu,e} = \frac{G_F^2 E m_e}{\pi} (1 - 4 \sin^2 \theta_W + \frac{16}{3} \sin^4 \theta_W)$$

and

$$\sigma^{\bar{\nu},e} = \frac{G_F^2 E m_e}{\pi} (\frac{1}{3} - \frac{4}{3} \sin^2 \theta_W + \frac{16}{3} \sin^4 \theta_W) .$$

These reactions can also serve to test this theory and have the advantage that strongly interacting particles are not involved, so that the understanding of strong-interaction corrections is not necessary in the interpretation. They have the experimental disadvantage of low rates and consequent large background. The best results at present are from a BNL experiment (Ahrens *et al.*, 1985) using relatively low-energy neutrinos, $E \approx 1.5$ GeV, and a 140-ton detector entirely composed of many layers of plastic scintillator and drift chambers. The background is subtracted on the basis of the distribution in the production angle of the electron shower (see Fig. 11). Instead of comparing the neutrino and antineutrino cross sections directly with the theory, the authors form the ra-

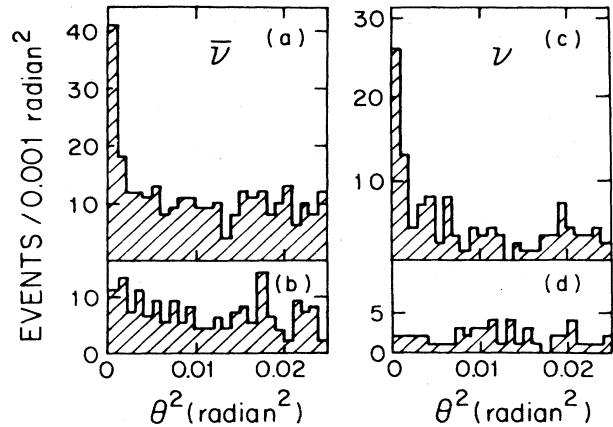


FIG. 11. Identification of neutrino-electron events on the basis of their small angle with respect to the beam in the experiment of Ahrens *et al.* (1985). The peak at small angles in the two top graphs is due to neutrino-electron scattering. The bottom graphs show the flat distribution observed if photons rather than electrons are detected. This shows the angular distribution of background events.

tio of the two, which is less sensitive to some systematic errors. From this they find the result $\sin^2 \theta_W = 0.209 \pm 0.032$. A CERN group reports a similar result (Dorenbosch *et al.*, 1988) with $\sin^2 \theta_W = 0.211 \pm 0.037$. The agreement with other methods of obtaining this angle is an important confirmation of the theory. A massive experiment to improve the precision is currently under way at CERN.

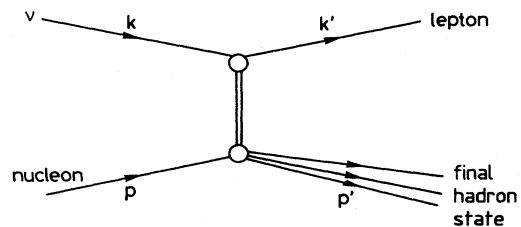
5. NEUTRINO-NUCLEON INCLUSIVE SCATTERING AND THE QUARK-STRUCTURE OF HADRONS

5.1 Phenomenology

We consider the CC reactions

$$\nu + N \rightarrow \mu^- + \text{hadrons} \quad \text{and} \quad \bar{\nu} + N \rightarrow \mu^+ + \text{hadrons}$$

independently of the final hadron configuration. This is called the inclusive process. It is assumed that the lepton vertex is described by the vector-axial-vector current of the electroweak theory. Let k be the initial and k' the final lepton energy-momentum four vectors, p that of the incident nucleon, and p' that of the final hadron state:



Define the kinematic variables

$$Q^2 \equiv -(k - k')^2 = 4EE' \sin^2 \theta / 2 ,$$

$$\nu \equiv pQ^2 / m_p = E_h - m_p \simeq E_h$$

(the energy of the final-state hadrons in the laboratory system),

$$x \equiv Q^2 / 2m_p \nu , \quad 0 \leq x \leq 1 ,$$

$$y \equiv \nu / E \simeq E_h / E , \quad 0 \leq y \leq 1 ,$$

where E and E' are the energies of the initial neutrino and final muon, respectively, and θ is the angle between these, all in the laboratory system. The cross sections can be written in terms of three structure functions, each a function of the variables x and Q^2 that characterize the hadronic vertex:

$$\frac{d^2 \sigma^{\nu(\bar{\nu})}}{dx dy} = \frac{G^2 m_p E_\nu}{2\pi} \{ F_2(x, Q^2) [1 + (1-y)^2] - y^2 F_L(x, Q^2)_{(-)}^+ x F_3(x, Q^2) \times [1 - (1-y)^2] \} .$$

The functions $F_2(x, Q^2)$, $x F_3(x, Q^2)$, and $F_L(x, Q^2)$ are the three structure functions that express what happens at the hadron vertex. The sum of neutrino and antineutrino cross sections has the same structure-function dependence as does the cross section for charged leptons:

$$\frac{d^2 \sigma^{l^\pm}}{dx dy} = \frac{2\pi \alpha^2 m_p E}{Q^4} \{ F_2^{l^\pm}(x, Q^2) [1 + (1-y)^2] - y^2 F_L(x, Q^2) \} .$$

5.2 Quark structure of the nucleon

In 1969, at the newly completed two-mile linear electron accelerator at SLAC, it was discovered (Bloom *et al.*, 1969, 1970; Breidenbach *et al.*, 1969) that in electron-proton collisions, at high momentum transfer, the form factors were independent of Q^2 . This so-called “scaling” behavior is characteristic of “point,” or structureless, particles. The interpretation in terms of a composite structure of the protons—that is, protons composed of pointlike quarks—was given by Bjorken (1969) and Feynman (1972).

Neutrinos are projectiles *par excellence* for investigating this structure, in part because of the heavy mass of the intermediate boson and in part because quarks and antiquarks are scattered differently by neutrinos owing to the $V - A$ character of the weak currents; they can therefore be distinguished in neutrino scattering, whereas in charged-lepton scattering this is not possible. The quark model makes definite predictions for neutrino-hadron scattering, which are beautifully confirmed experimentally. Many of the predictions rest on the fact that now the kinematical variable x takes on a physical meaning: it can be interpreted as the fraction of the nucleon momentum or mass carried by the quark on which the scattering

takes place. The neutrino experiments we review here have primarily used iron as the target material. Iron has roughly equal numbers of protons and neutrons. For such nuclei, the cross sections can be expressed in terms of the total quark and total antiquark distributions in the proton. Let $u(x)$, $d(x)$, $s(x)$, $c(x)$, etc., be the up, down, strange, charm, etc., quark distributions in the proton. The proton contains three “valence” quarks: two up quarks and one down quark. In addition, it contains a “sea” of virtual quark-antiquark pairs. The up-valence-quark distribution is $u(x) - \bar{u}(x)$, and the down-valence-quark distribution is $d(x) - \bar{d}(x)$. The sea quarks and antiquarks have necessarily identical distributions, so that $s(x) = \bar{s}(x)$, $c(x) = \bar{c}(x)$, etc. For the neutron, u and d change roles, but s and c are the same. Let

$$q(x) = u(x) + d(x) + s(x) + c(x) + \dots$$

and

$$\bar{q}(x) = \bar{u}(x) + \bar{d}(x) + \bar{s}(x) + \bar{c}(x) + \dots$$

be the total quark and antiquark distributions of the proton, respectively. For spin- $\frac{1}{2}$ quarks interacting according to the standard model, for a target with equal numbers of protons and neutrons, and for $Q^2 \ll m_W^2$ and $m_p \ll E$,

$$\frac{d^2 \sigma^\nu}{dx dy} = \frac{G_F^2 E m_p}{\pi} x [q(x) + (1-y)^2 \bar{q}(x)]$$

and

$$\frac{d^2 \sigma^{\bar{\nu}}}{dx dy} = \frac{G_F^2 E m_p}{\pi} x [\bar{q}(x) + (1-y)^2 q(x)] .$$

Comparison with the expression for the cross section in terms of structure functions then gives these functions in terms of quark distributions:

$$F_2(x, Q^2) = x [q(x) + \bar{q}(x)] ,$$

where $q(x) + \bar{q}(x)$ is the total quark + antiquark distribution;

$$x F_3(x, Q^2) = x [q(x) - \bar{q}(x)] ,$$

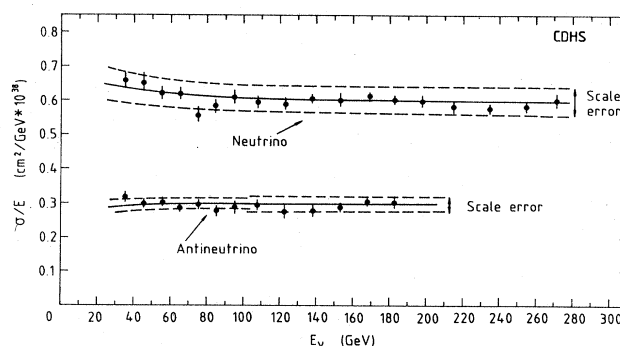


FIG. 12. Total neutrino and antineutrino cross sections per nucleon divided by neutrino energy. The flat “scaling” behavior is a consequence of the pointlike interaction of the constituents (de Groot *et al.*, 1979; Abramowicz *et al.*, 1982a, 1983, 1988).

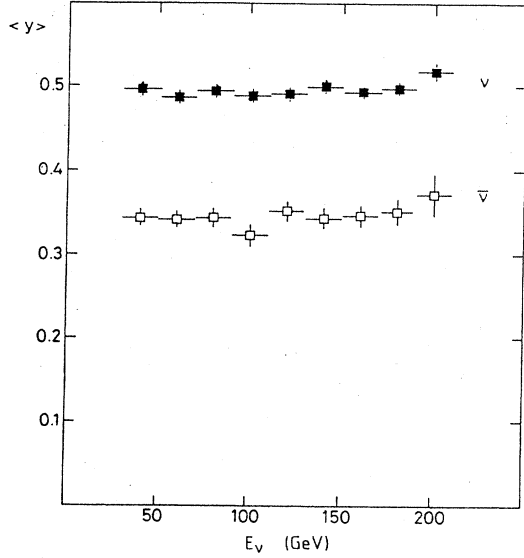


FIG. 13. The average of y (the fraction of the neutrino energy transmitted to the final hadron state) as a function of the neutrino energy, for neutrinos and antineutrinos. The uniformity is a consequence of scaling, which in turn is a consequence of the pointlike interaction of the quark (de Groot *et al.*, 1979; Abramowicz *et al.*, 1982a, 1983, 1988).

where $q(x) - \bar{q}(x)$ is the valence-quark distribution; and

$$F_L(x, Q^2) = 0,$$

a consequence of the spin- $\frac{1}{2}$ nature of the quarks.

From these simple expressions for the cross sections, in terms of quark structure, several tests of the quark model are derived. For the experimental comparisons, we take the CDHS experiments (de Groot *et al.*, 1979; Abramowicz *et al.*, 1982a, 1983, 1988). It should be noted that the measurements in the detector, i.e., the hadron energy and the muon momentum, are just sufficient to define the inclusive process.

(1) *Scaling.* The independence of the differential cross sections with respect to Q^2 is evident everywhere, over a large domain in Q^2 . As one example, Fig. 12 shows the linearity of the total cross sections with neutrino energy; as another, Fig. 13 shows the uniformity of the average of y with respect to neutrino energy; both examples are consequences of scaling. Small deviations from scaling are observed in the structure functions, as we shall see later, but these have their explanation in the strong interactions of the quarks.

(2) *The y dependence of the cross sections.* We expect

$$\frac{d\sigma^\nu}{dy} + \frac{d\sigma^{\bar{\nu}}}{dy} \propto [1 + (1-y)^2] \int x [q(x) + \bar{q}(x)] dx$$

and

$$\frac{d\sigma^\nu}{dy} - \frac{d\sigma^{\bar{\nu}}}{dy} \propto [1 - (1-y)^2] \int x [q(x) - \bar{q}(x)] dx .$$

The agreement with this expectation is quite good, as can be seen from Fig. 14. A corollary of this agreement is that $F_L(x)$ is small. It is found that $\int F_L(x) dx / \int F_2(x) dx \simeq 0.1$. Again, this deviation from the simple

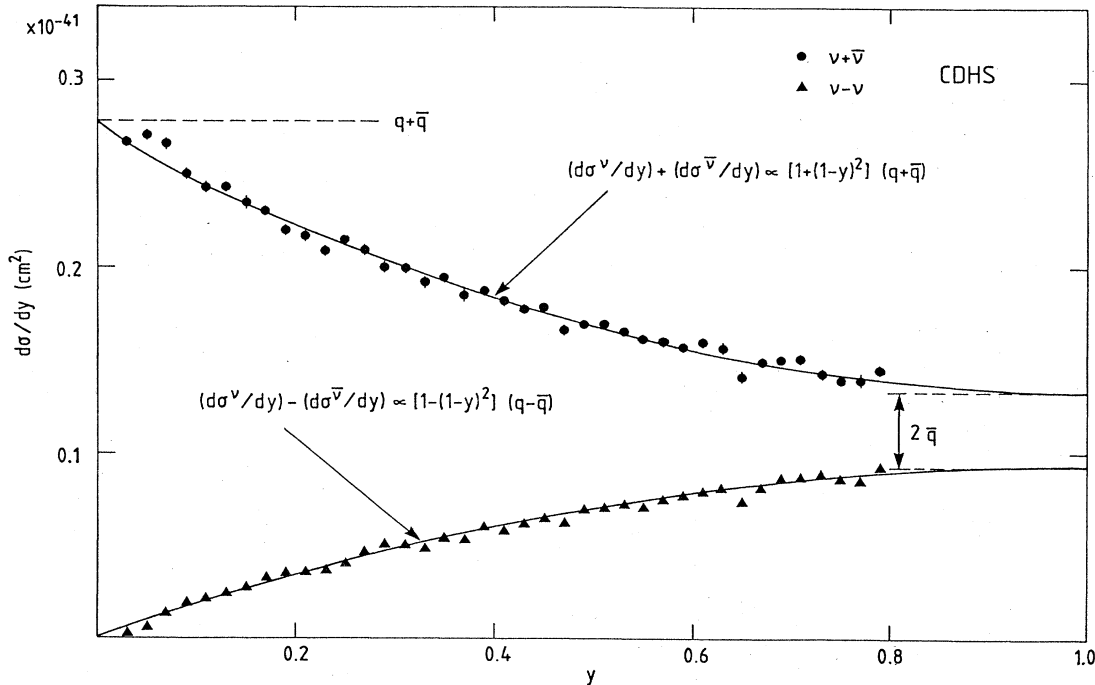


FIG. 14. The y dependence of the sum and the difference of neutrino and antineutrino cross sections. Spin- $\frac{1}{2}$ quarks are expected to have y dependences $1 + (1-y)^2$ for the sum and $1 - (1-y)^2$ for the difference (de Groot *et al.*, 1979; Abramowicz *et al.*, 1982a, 1983, 1988).

quark picture is understood in terms of the strong interactions of the quarks, as we shall see later.

(3) *Correspondence between $F_2^{l\pm}(y)$ and $F_2^{\nu}(x)$.* Both are proportional to $q(x) + \bar{q}(x)$, and so are expected to have the same x dependence in the simple quark model. They are related by the factor

$$\frac{F_2^{l\pm}(x)}{F_2^{\nu}(x)} = \frac{1}{2} \left[\left(\frac{2}{3}\right)^2 + \left(-\frac{1}{3}\right)^2 \right] = \frac{5}{18}.$$

Here $\frac{2}{3}$ and $-\frac{1}{3}$ are the up- and down-quark electric charges, respectively. The agreement in shape and magnitude, shown in Fig. 15, not only supports the quark picture but also demonstrates the third integral quark electric charges.

(4) $\int xF_3(x)dx/x = 3$. Since $xF_3(x) = x[q(x) - \bar{q}(x)]$ in the quark model and $q(x) - \bar{q}(x)$ is the valence-quark distribution, this sum rule states that there are three valence quarks in the nucleon. The experimental demonstration is not without problems, because the ν and $\bar{\nu}$ cross sections are finite as $x \rightarrow 0$, and the difference, which is $xF_3(x)$, has a consequent large error at small x , which is divided by x as $x \rightarrow 0$. However, all experiments give a value near 3, with typical uncertainties of $\sim 10\%$.

Together with the charged-lepton inclusive scattering experiments, the neutrino experiments leave no doubt about the validity of the quark picture of nucleon structure. In addition, the neutrino experiments are unique in offering the possibility of measuring independently the quark and antiquark distributions in the nucleon, shown in Fig. 15.

If the quarks were the sole nucleon constituents, we would expect $\int F_2 dx = \int x[q(x) + \bar{q}(x)] dx$ to be equal to 1. Experimentally, $\int F_2(x) dx = 0.48 \pm 0.02$. We should have expected that some of the nucleon momen-

tum would be carried by the gluons, the mesons that bind the quarks. The experimental result is therefore interpreted to mean that gluons account for about half of the nucleon momentum (or mass).

5.3 Neutrino scattering and quantum chromodynamics (QCD)

QCD is the elegant new gauge theory of the interaction of quarks and gluons, which describes the binding of quarks into the hadrons. Deep-inelastic lepton scattering provided a means of testing the predictions of this important theory and gave it its first experimental support. So far, no one has succeeded in calculating low-energy hadronic phenomena such as the wave functions of quarks in hadrons, because of the large coupling constant that frustrates perturbation methods at low energy. At high Q^2 , however, the effective coupling constant becomes logarithmically smaller, and perturbation calculations become credible. The theory predicts "scaling violations" in the form of a "shrinking" of the structure functions towards smaller x as Q^2 gets larger. This is observed experimentally, as can be seen from Fig. 16. In the theory, the "shrinking" is the consequence of the emission of gluons in the scattering process. This emission can be calculated. The Q^2 evolution at sufficiently high Q^2 is therefore quantitatively predicted by the theory. In neutrino experiments, this Q^2 evolution could be measured,

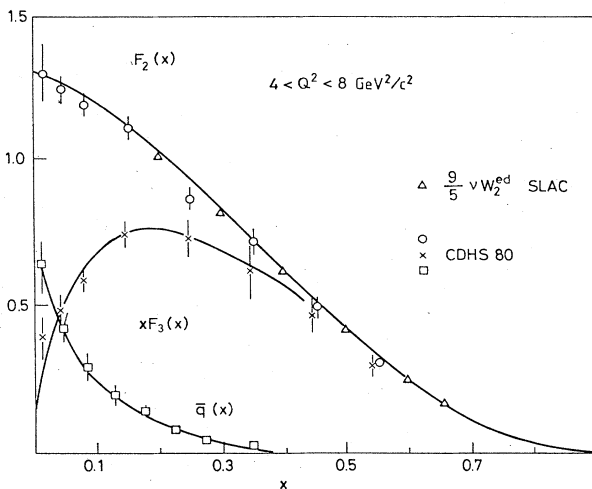


FIG. 15. The structure functions $xF_3(x)$, $F_2(x)$, and $\bar{q}(x)$. In the simple quark picture $F_2(x) = x[q(x) + \bar{q}(x)]$ and $xF_3(x) = x[q(x) - \bar{q}(x)]$.

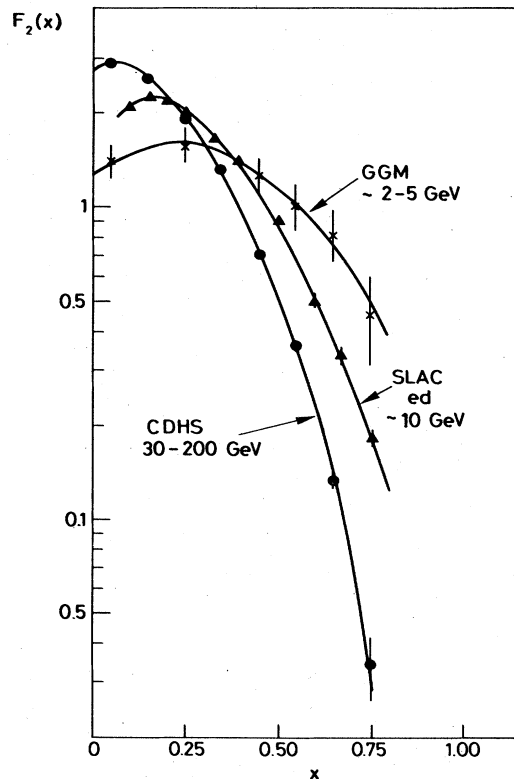


FIG. 16. Scaling is only approximately true for the structure functions. Early measurements of $F_2(x)$ in three different energy domains exhibit shrinking, as expected in the QCD theory.

and these measurements confirmed the theory and contributed to its acceptance. In the case of xF_3 , the theoretical predictions have only one free parameter, the coupling constant α_s . In the case of F_2 , the Q^2 evolution is coupled to the gluon distribution $G(x, Q^2)$. The experimental Q^2 evolutions of xF_3 and F_2 in the latest CDHS experiment are shown, together with their QCD fits, in

Figs. 17 and 18. The theory fits the data adequately. These fits give a value for the parameter Λ in the running strong-coupling constant,

$$\alpha_s = [6 / (33 - 2N_f) \ln(Q^2 / \Lambda^2)] ,$$

where N_f = number of excited quark flavors ($N_f \approx 4$ in this experiment), $\Lambda \approx 100$ MeV. They also give the gluon distribution shown in Fig. 19. These QCD comparisons suffer somewhat from the fact that Q^2 is still too low to reduce nonperturbative effects to a negligible level, but

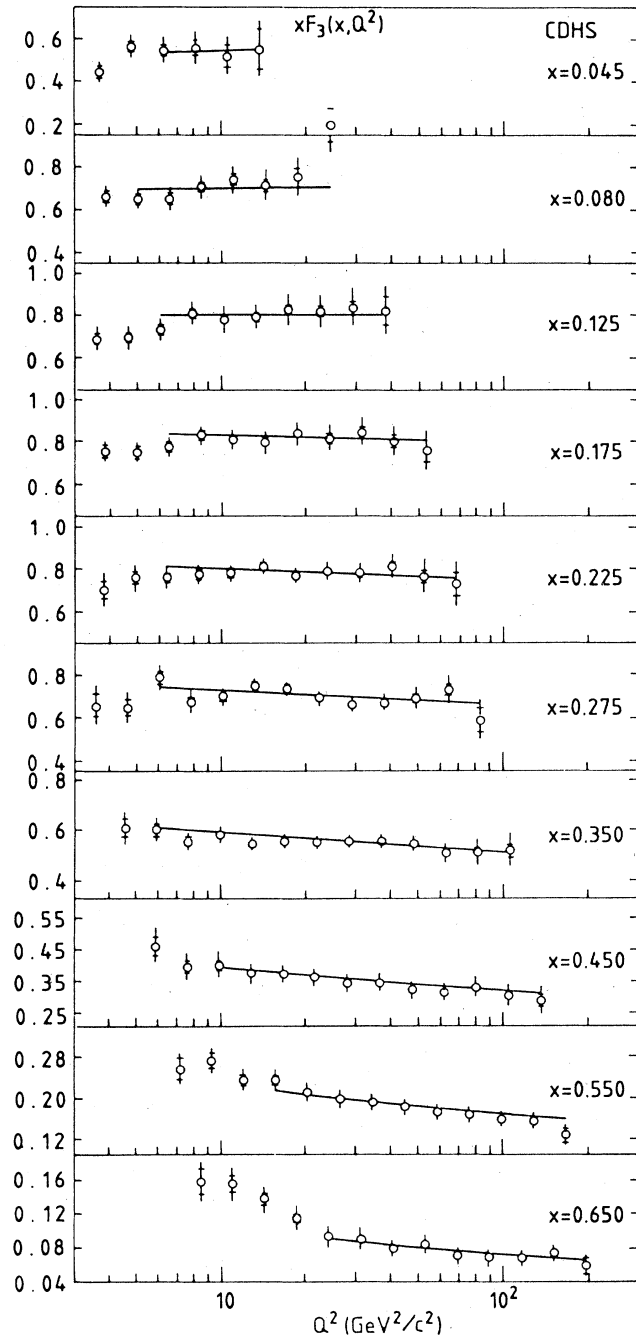


FIG. 17. Variation of $xF_3(x, Q^2)$ with $\ln Q^2$ in different x bins. The Q^2 evolution predictions of QCD with $\Lambda = 128$ MeV are also shown (de Groot *et al.*, 1979; Abramowicz *et al.*, 1982a, 1983, 1988).

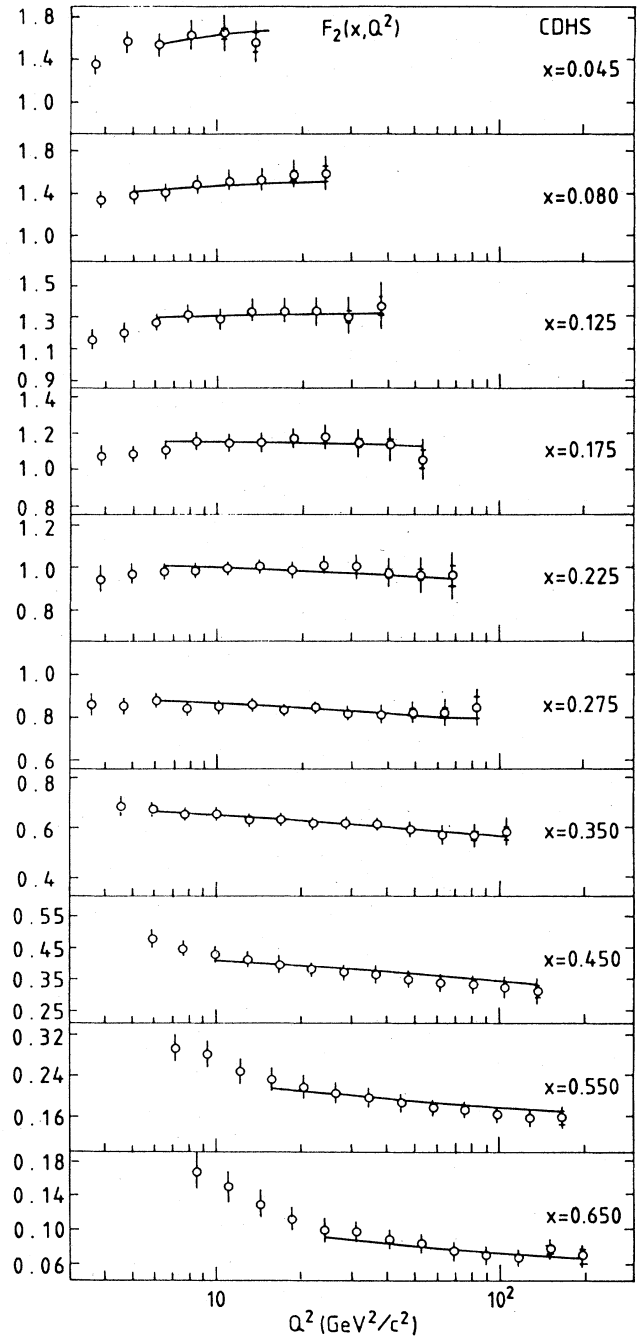


FIG. 18. Variation of $F_2(x, Q^2)$ with $\ln Q^2$. The QCD fit is also shown.

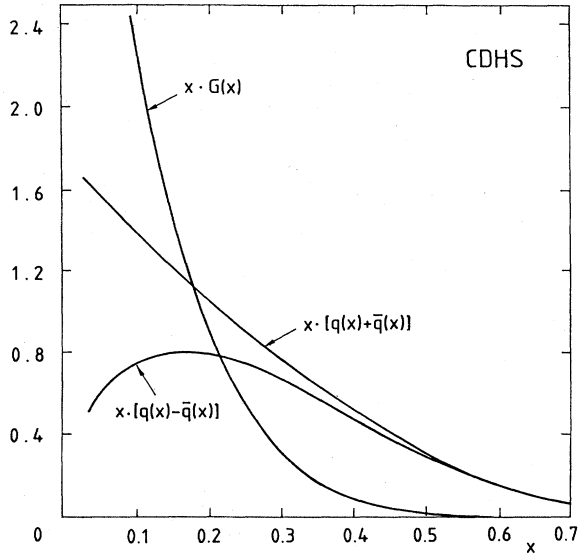


FIG. 19. The gluon distribution $G(x)$ derived from the QCD fits to $F_2(x, Q^2)$, $\bar{q}(x, Q^2)$, and $xF_3(x, Q^2)$ (de Groot *et al.*, 1979; Abramowicz *et al.*, 1982a, 1983, 1988).

the calculable perturbative effects dominate and are confirmed by the experiments. Perturbative QCD also predicts a nonzero longitudinal structure function $F_L(x, Q^2)$ as another consequence of the emission of gluons. This prediction is compared with the CDHS experimental results in Fig. 20. Again, the experiment lends support to the theory.

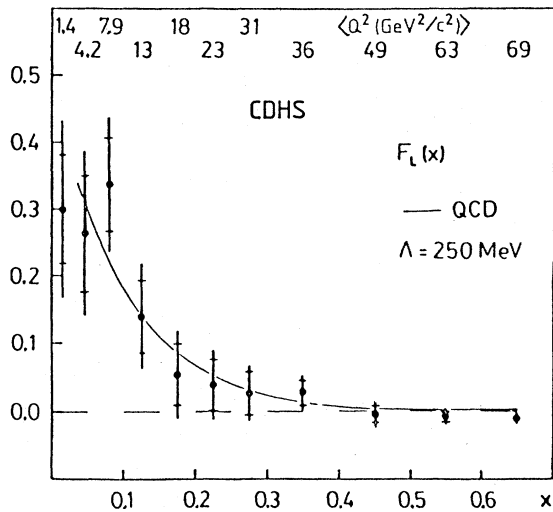


FIG. 20. The structure function $F_L(x)$ associated with longitudinally polarized intermediate bosons, and the QCD predictions. In the simple quark model, F_L is zero (de Groot *et al.*, 1979; Abramowicz *et al.*, 1982a, 1983, 1988).

6. NEUTRINO INTERACTIONS, THE GIM WEAK CURRENT, AND THE STRANGE QUARK IN THE NUCLEON

Among the most beautiful results obtained with neutrino beam experiments are those concerning the opposite-sign “dimuons” first observed at Fermilab (Benvenuti *et al.*, 1975) and studied in detail in the CDHS experiments (Holder *et al.*, 1977a; Abramowicz *et al.*, 1982b). These reactions occur with roughly $\frac{1}{100}$ of the rate of the dominant single-muon events. The experiments are interesting, on the one hand because they confirm the doublet structure of the quark weak current proposed some years ago by Glashow, Iliopoulos, and Maiani (1970), and which is fundamental to the electroweak theory, and on the other hand because they give such a vivid confirmation of the nucleon quark structure altogether.

The origin of the extra muon was quickly understood as being due to the production of charmed quarks and their subsequent muonic decay. In the Glashow-Iliopoulos-Maiani (GIM) model, the charm-producing reactions are

GIM cross-section proportionality

$$\nu + d \rightarrow \mu^- + c, \quad c \rightarrow \mu^+ + \dots, \quad x d(x) \sin^2 \theta_C, \quad (3)$$

$$\nu + s \rightarrow \mu^- + c, \quad c \rightarrow \mu^+ + \dots, \quad x s(x) \cos^2 \theta_C, \quad (4)$$

and

$$\bar{\nu} + \bar{d} \rightarrow \mu^+ + \bar{c}, \quad \bar{c} \rightarrow \mu^- + \dots, \quad x \bar{d}(x) \sin^2 \theta_C, \quad (5)$$

$$\bar{\nu} + \bar{s} \rightarrow \mu^+ + \bar{c}, \quad \bar{c} \rightarrow \mu^- + \dots, \quad x \bar{s}(x) \cos^2 \theta_C. \quad (6)$$

The identification of the extra muon events with charm decay is experimentally confirmed in a number of ways.

- (i) Opposite-sign muons are produced, like-sign ones are not.
- (ii) In general, the extra muon has little energy.
- (iii) The extra muon is correlated, as expected, to the direction of the hadron shower, of which the charmed particle is a part.

The GIM paper (Glashow, Iliopoulos, and Maiani, 1970) preceded the experimental discovery of charm by five years. It was proposed because of the theoretical attractiveness of the doublet structure of the weak currents. The predictions were precise. The cross sections are proportional to $\sin^2 \theta_C$ for d and \bar{d} quarks and to $\cos^2 \theta_C$ for s and \bar{s} quarks. The Cabibbo angle θ_C was previously known, with $\cos^2 \theta_C = 0.97$, close to 1, and $\sin^2 \theta_C = 0.05$, very much smaller. Reactions (3) and (4), or (5) and (6), are not experimentally separable, since the target nucleon contains both s and d quarks, and the final state is the same. In the antineutrino case, reaction (6) dominates (5) because $\sin^2 \theta_C$ is so small. For each event, x and y are measured as for single-muon events. Therefore the x distribution for antineutrino dimuon production, shown in

Fig. 21(a), measures the amount and the shape of the strange sea $s(x)$.

In the neutrino reactions, the smallness of $\sin^2\theta_C$ for reaction (3) is very closely compensated by the fact that $d(x)$, containing also valence quarks, is much greater than $s(x)$ of reaction (4). By fitting, it can be seen that the x distribution in Fig. 21(b) is a roughly equal mixture of $s(x)$ as obtained with the antineutrinos and $d(x)$, previously known from the normal CC reactions. The ratio of the two contributions is a measure of θ_C as it enters the charm production reaction. The Cabibbo angle obtained in this way is found to be equal, within errors, to θ_C measured in strange decays, as proposed in the GIM

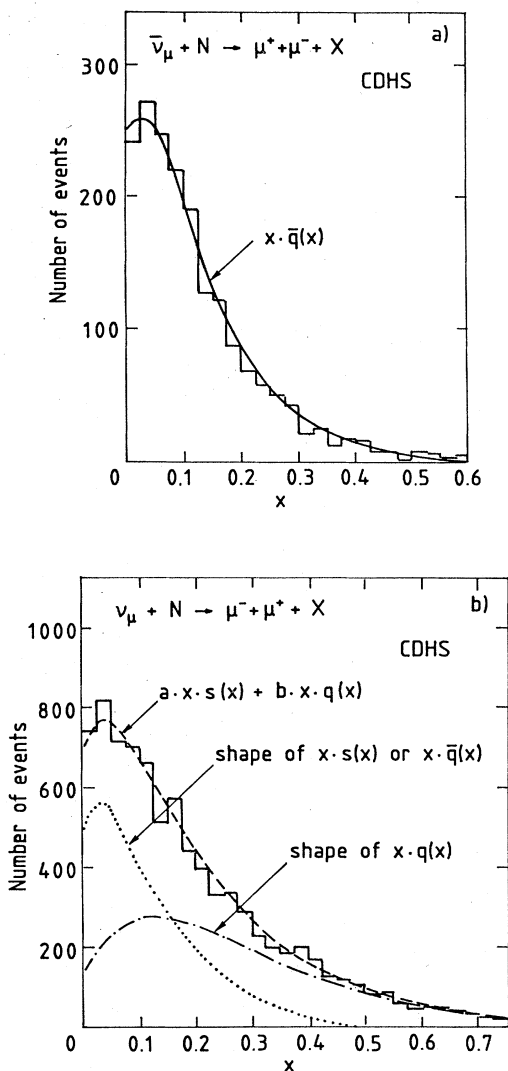


FIG. 21. The x distributions of opposite-sign dimuon events: (a) for antineutrinos. The dominant process is $\bar{\nu} + \bar{s} \rightarrow \mu^+ + \bar{c}$. The observed x distribution is therefore that of the strange sea in the nucleon. (b) for neutrinos. The process is $\nu + s$ or $d \rightarrow \mu^- + c$. The shape allows the determination of the relative contributions of s and d quarks, and therefore the relative coupling constant. This confirmed the GIM prediction (Holder *et al.*, 1977a; Abramowicz *et al.*, 1982b).

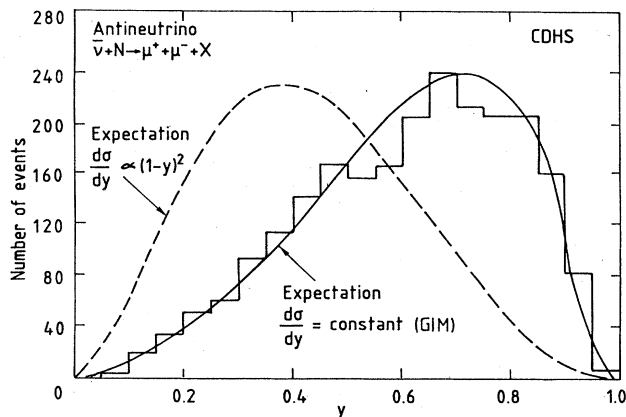


FIG. 22. The y distribution of $\bar{\nu}$ -produced dimuons. The acceptance over the y domain is unfortunately very nonuniform, because of the 5-GeV minimum energy required of each muon. The observed y distribution agrees with an acceptance-corrected flat y distribution as predicted by the GIM current, but differs strikingly from the $(1-y)^2$ distribution characteristic of the single-muon antineutrino cross section (Holder *et al.*, 1977a; Abramowicz *et al.*, 1982b).

hypothesis. Further support of the GIM current is provided by the y distributions. They reflect the relative helicities of the neutrino and the struck quark: if the two helicities are the same, as is the case for all four charm-producing reactions, the expected y distribution is flat; if they are opposite, as is the case for instance for $\nu + \bar{q}$ and $\bar{\nu} + q$, the expected distribution is $(1-y)^2$. Both neutrino and antineutrino single-muon reactions are mixtures of the two, as we saw in Fig. 14. The contrast is especially strong for antineutrinos, where the experimental single-muon y distribution is dominated by $(1-y)^2$, whereas the dimuon distribution is flat, as shown in Fig. 22, again confirming the GIM picture.

7. CONCLUDING REMARKS

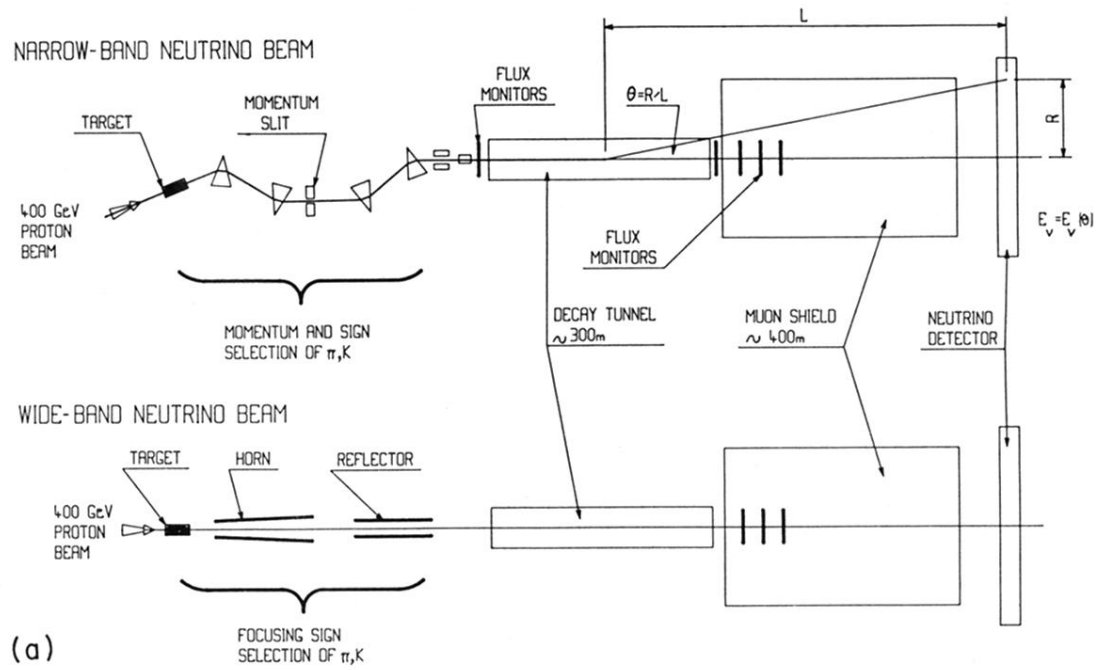
I have given some examples to illustrate the impact of high-energy neutrino research on the particle physics progress of the past years, both in the field of the weak interactions and in that of nucleon structure. How will this develop in the future? I do not know, of course. The increase of proton accelerator energies into the 10-TeV range will certainly permit better QCD tests than those cited above. In general, however, it can be expected that progress in particle physics will depend more and more on colliders, because of their higher center-of-mass energies. High-energy $e-p$ machines, such as HERA, will permit exploration of inclusive scattering to higher Q^2 domains than will be possible with fixed-target neutrino beams.

However, the fascination with neutrinos and the unanswered questions concerning them—such as their masses—are motivating a broad line of research in astro-

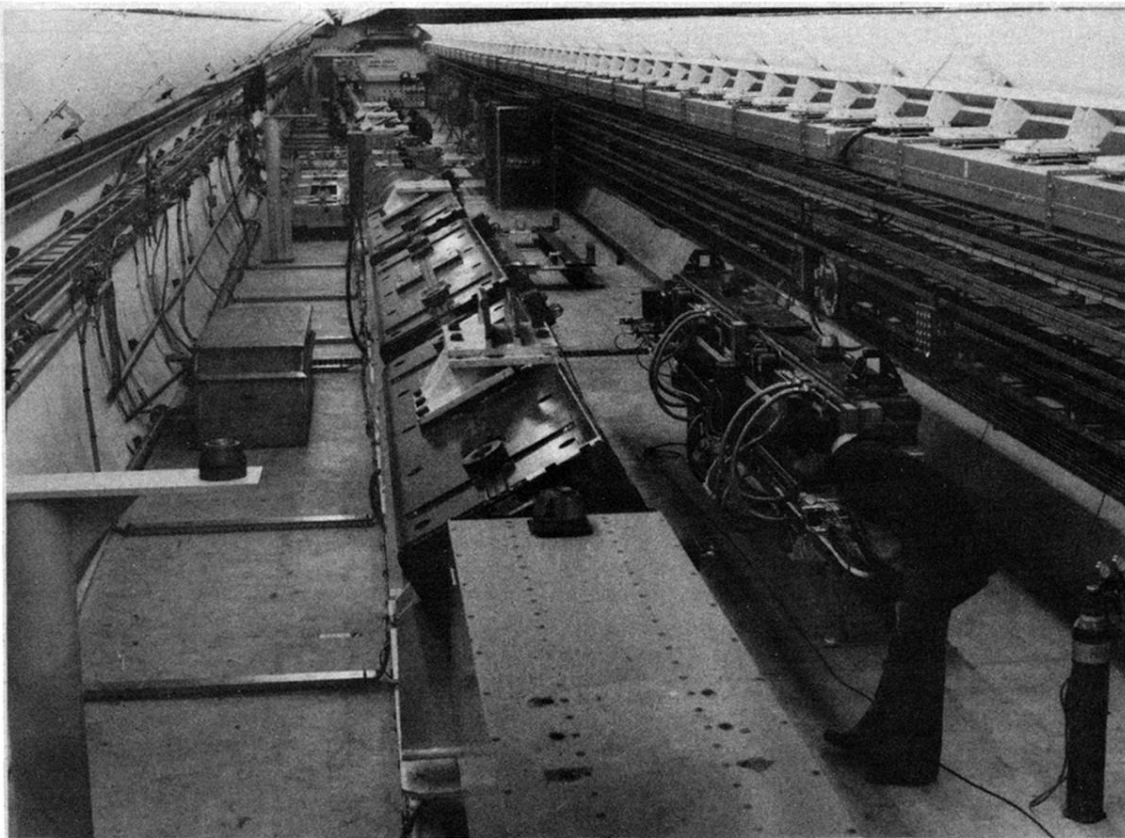
physics, accelerator physics, and nuclear physics. One of the first and most important results expected from the two large e^+e^- colliders just coming into operation, the Stanford Linear Collider and the CERN LEP, which will produce lots of Z^0 mesons, is the determination of how many families of leptons and quarks there really are. Are there others besides the three already known? This fundamental question will be answered by determining how often the Z^0 decays to neutrinos, even if the masses of the other members of possible additional families are too large to permit their production at these energies.

REFERENCES

- Abramowicz, H., *et al.*, 1982a, *Z. Phys. C* **12**, 289.
 Abramowicz, H., *et al.*, 1982b, *Z. Phys. C* **15**, 19.
 Abramowicz, H., *et al.*, 1983, *Z. Phys. C* **17**, 283.
 Abramowicz, H., *et al.*, 1985, *Z. Phys. C* **28**, 51.
 Abramowicz, H., *et al.*, 1986, *Phys. Rev. Lett.* **57**, 298.
 Abramowicz, H., *et al.*, 1988, "A measurement of differential cross sections and nucleon structure functions in charged-current neutrino interactions on iron," unpublished.
- Ahrens, L. H., *et al.*, 1985, *Phys. Rev. Lett.* **54**, 18.
 Benvenuti, A., *et al.*, 1975, *Phys. Rev. Lett.* **34**, 419.
 Bjorken, J. D., 1969, *Phys. Rev.* **179**, 1547.
 Bloom, E. D., *et al.*, 1969, *Phys. Rev. Lett.* **23**, 930.
 Bloom, E. D., *et al.*, 1970, "Recent results in inelastic electron scattering," Stanford Report No. SLAC-PUB 796, 1970 (unpublished), paper 7b-17 submitted to the 15th International Conference on High-Energy Physics, Kiev, 1970. See, in *Proceedings* (Naukova Dumka, Kiev, 1972), the talk by R. Wilson, p. 238.
 Breidenbach, M. L., J. I. Friedman, H. W. Kendall, E. D. Bloom, D. H. Coward, H. DeStaebler, J. Drees, L. W. Mo, and R. E. Taylor, 1969, *Phys. Rev. Lett.* **23**, 935.
 de Groot, J. G. H., *et al.*, 1979, *Z. Phys. C* **1**, 143.
 Dorenbosch, J., *et al.*, 1988, *Z. Phys. C* (in press).
 Feynman, R. P., 1972, *Photon-Hadron Interactions* (Benjamin, Reading, Massachusetts).
 Glashow, S. L., J. Iliopoulos, and L. Maiani, 1970, *Phys. Rev. D* **2**, 1285.
 Hasert, F. J., *et al.*, 1973a, *Phys. Lett. B* **46**, 121.
 Hasert, F. J., *et al.*, 1973b, *Phys. Lett. B* **46**, 138.
 Holder, M., *et al.*, 1977a, *Phys. Lett. B* **69**, 377.
 Holder, M., *et al.*, 1977b, *Phys. Lett. B* **71**, 222.
 Holder, M., *et al.*, 1977c, *Phys. Lett. B* **72**, 254.



(a)



(b)

FIG. 1. (a) Sketch of narrow-band and wide-band neutrino beam layouts at CERN, showing disposition of primary target, focusing elements, decay region, shielding, and monitoring devices. (b) View of the neutrino beam tunnel at the CERN SPS in 1976, before operations began. The NBB line is seen in the center; on the right is the pulse transformer for the WBB horn, but the horn itself, destined for the pedestal on the left, is not yet installed. At the far end, the 2.5-m-diameter titanium window of the evacuated decay region can be seen. Photograph by PHOTO CERN.

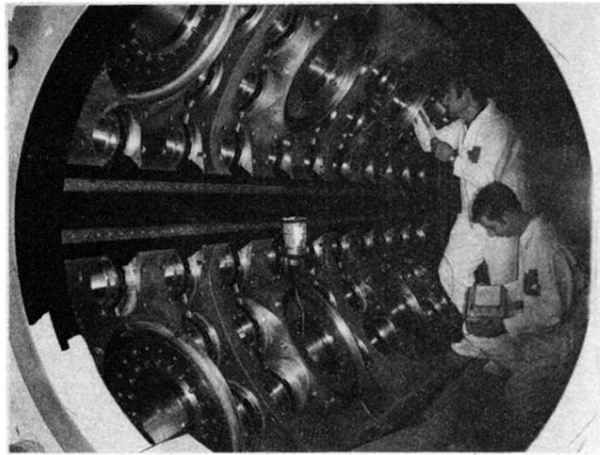


FIG. 4. Preparation of the interior of the 13-m³ bubble chamber Gargamelle, later to be filled with Freon. It is with this detector that the neutral currents were discovered. Photograph by PHOTO CERN.

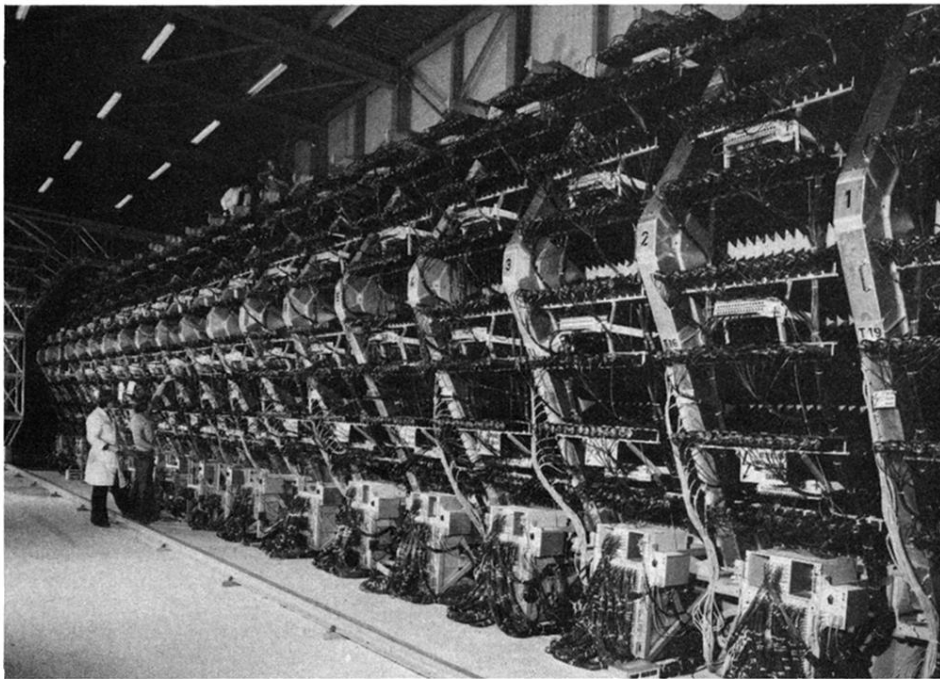


FIG. 5. View along the 19 modules of the CDHS electronic neutrino detector at the SPS. The black light-guides and phototubes, which are used to measure the hadron energy, can be seen sticking out of the magnetized iron modules. The hexagonal aluminum structures are the drift chambers that measure the muon trajectories. Photograph by PHOTO CERN.

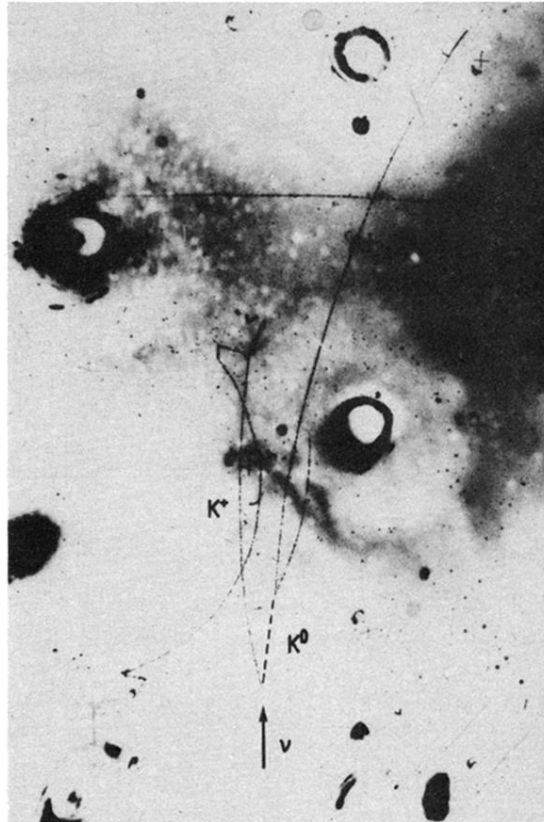


FIG. 7. A "muonless" event in Gargamelle. All tracks stop or interact in the chamber. None could be a muon. The neutrino produces one K^+ and one K^0 meson. The K^+ meson interacts in the liquid and then decays. The invisible K^0 meson decays to two pions.